Influence of entrainment on the thermal stratification in simulations of radiative-convective equilibrium

Martin S. Singh[1] and Paul A. O'Gorman[1]

Received 2 July 2013; revised 24 July 2013; accepted 26 July 2013; published 27 August 2013.

[1] Convective available potential energy (CAPE) is shown to increase rapidly with warming in simulations of radiative-convective equilibrium over a wide range of surface temperatures. The increase in CAPE implies a systematic deviation of the thermal stratification from moist adiabatic that is non-negligible at high temperatures. However, cloud buoyancy remains much smaller than what CAPE would imply because entrainment is more effective in reducing buoyancy in warmer atmospheres. An entraining plume model in the limit of zero cloud buoyancy is shown to reproduce the increase in CAPE with warming if the entrainment rate is held fixed and increases in the vertical extent of convection are taken into account. These model results together with radiosonde observations are used to support a conceptual model in which entrainment plays a role in determining the thermal stratification of the tropical atmosphere. **Citation:** Singh, M. S., and P. A. O'Gorman (2013), Influence of entrainment on the thermal stratification in simulations of radiative-convective equilibrium, *Geophys. Res. Lett.*, *40*, 4398–4403, doi:10.1002/grl.50796.

1. Introduction

[2] Convective available potential energy (CAPE), defined as the integrated buoyancy experienced by an undilute parcel as it rises to its level of neutral buoyancy (LNB), is a common measure of the deviation of the atmospheric thermal stratification from that of an undilute moist adiabat. CAPE over the tropical oceans has been found to increase rapidly in climate-model simulations of global warming, with increases of up to 25% occurring in projections of 21st century climate [*Sobel and Comargo*, 2011; *Fasullo*, 2012]. CAPE also increases with warming in simulations of radiative-convective equilibrium (RCE) performed using cloud-system resolving models (CRMs) [*Muller et al.*, 2011; *Romps*, 2011]. Despite the robustness of this result, it is not clear why the CAPE increases with temperature or what the implications for updraft velocities and precipitation intensity may be.

[3] In this study, we show that the increase in CAPE with warming occurs over a wide range of temperatures in simulations of RCE with different CO_2 concentrations. Consistent with previous work [*Muller et al.*, 2011], typical buoyancies found inside clouds are much smaller than those associated with the undilute parcels used to define CAPE. This suggests that entrainment of dry air may be important in setting cloud buoyancy. Motivated by the relative smallness of the cloud buoyancy, we show that the increase in CAPE with warming can be accounted for using a conceptual model in which the atmosphere remains close to neutrally buoyant with respect to an entraining plume with a fixed entrainment profile. The extent to which entrainment reduces the plume buoyancy depends on the saturation deficit of the midtroposphere, and this saturation deficit increases with warming if the relative humidity remains roughly constant. The greater CAPE in a warmer atmosphere then results from a greater difference in temperature between the entraining plume and the undilute parcel used in the calculation of CAPE.

[4] The conceptual model outlined here is consistent with the convective quasi-equilibrium hypothesis as described by *Arakawa and Schubert* [1974] in which it is argued that moist convection constrains the "cloud work-function" (a plume-based counterpart to CAPE that considers entrainment) to be close to zero. A role for entrainment in helping to determine cloud buoyancies in moist convection is supported by CRM simulations and some observational studies [e.g., *Derbyshire et al.*, 2004; *Holloway and Neelin*, 2009; *Kuang and Bretherton*, 2006; *Romps and Kuang*, 2010; *Zipser*, 2003; *Molinari et al.*, 2012]. Others, however, have argued for the importance of undilute ascent in maintaining the mean thermodynamic structure of the tropical atmosphere [e.g., *Riehl and Malkus*, 1958; *Xu and Emanuel*, 1989], and it is unclear whether current models adequately represent the relevant mixing processes. Thus, we also provide observational support for the conceptual model discussed above by showing it is consistent with observed lapse rates from radiosondes in the tropical western Pacific; drier soundings (greater saturation deficit) allow for greater CAPE in a manner consistent with the plume model used to account for the CRM results.

[5] We begin by describing the CRM simulations and the CAPE of the mean profiles (section 2). We then introduce a simple bulk entraining plume model in the limit of zero buoyancy that accounts for the CRM results and which highlights the importance of midtropospheric humidity in modulating the effect of entrainment (section 3). We also present observational evidence for a relationship between tropospheric humidity and lapse rate; this evidence suggests the mechanisms found in the CRM and plume model are relevant to the atmosphere (section 4). Finally, we give a summary of our conclusions and their implications (section 5).

Additional supporting information may be found in the online version of this article.

[1]Department of Earth, Atmospheric and Planetary Sciences, Massachusetts Institute of Technology, Cambridge, Massachusetts, USA.

Corresponding author: M. S. Singh, Department of Earth, Atmospheric and Planetary Sciences, Massachusetts Institute of Technology, 77 Massachusetts Ave., Cambridge, MA 02139, USA. (mssingh@mit.edu)

0094-8276/13/10.1002/grl.50796

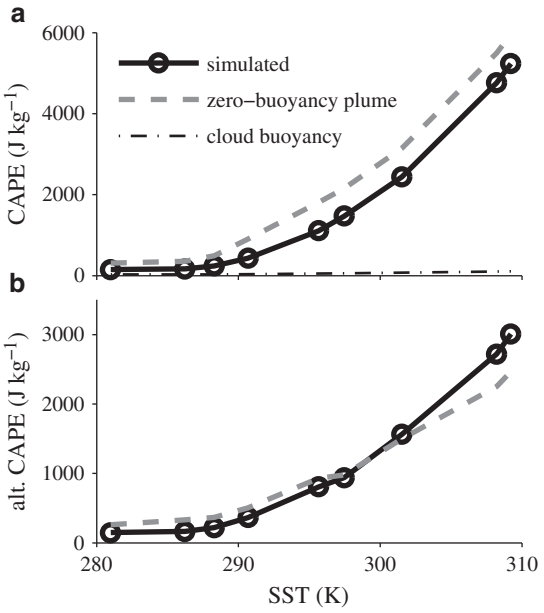

Figure 1. Pseudo-adiabatic CAPE in simulations of radiative-convective equilibrium (solid lines with circles) and as predicted by the zero-buoyancy plume model (dashed lines). CAPE is calculated by integrating positive parcel buoyancy up to (a) the LNB or alternatively (b) the anvil detrainment level. The anvil detrainment level is taken to be the level of maximum horizontal- and time-mean cloud-ice concentration in the simulations. The dash-dotted line in Figure 1a shows the cloud-buoyancy integral as defined in the text.

2. CAPE in a Cloud-System Resolving Model

[6] We describe results from three-dimensional simulations of radiative-convective equilibrium (RCE) over a wide range of sea surface temperatures (SSTs) and atmospheric CO_2 concentrations using version 16 of the Bryan Cloud Model [*Bryan and Fritsch*, 2002]. The model is fully compressible and nonhydrostatic and employs a Smagorinsky turbulence scheme to represent subgrid scale motions. Surface fluxes are parameterized by bulk aerodynamic formulae, with turbulent exchange coefficients calculated using Monin-Obukov similarity theory. Microphysics are treated using a six-species, one-moment scheme based on that of *Lin et al.* [1983]. A band-averaged radiative transfer scheme is used, and all simulations are performed with a constant solar flux of 390 W m^{-2} incident at a zenith angle of 43°.

[7] Nine simulations are conducted, each with a different imposed CO_2 concentration in the range 1–1280 ppmv and a corresponding SST between 286 and 309 K. The simulations are run with a horizontal grid spacing of 1 km in an 84×84 km doubly periodic domain for 40 days, with statistics collected over the last 20 days (Figure S1). The SST is fixed in each simulation and is chosen as the equilibrium SST in a corresponding lower-resolution slab-ocean simulation with the same atmospheric CO_2 concentration (Figure S2). Further details of the model and simulations are given in the supporting information (section S1).

[8] Figure 1a shows that the CAPE in the CRM simulations increases quasi-exponentially with SST. The same data are plotted with a logarithmic ordinate in Figure S3. CAPE is defined as the vertical integral of the positive buoyancy of a pseudo-adiabatic parcel lifted to its level of neutral buoyancy (LNB). (Similar behavior is found for reversible CAPE (Figure S4).) The buoyancy of the parcel is calculated relative to the domain- and time-mean virtual temperature profile, and the parcel is initialized with the mean temperature and specific humidity of the lowest model level. Ice is treated with a mixed phase over the range 233.15 to 273.15 K consistent with the CRM thermodynamics. The CAPE values range from less than 200 J kg^{-1} in the coldest simulation to more than 5000 J kg^{-1} in the warmest simulation. The increase in buoyancy of the undilute parcel is most pronounced in the upper troposphere, and there is also an important contribution from the increase in height of the LNB (Figure 2a). The fractional rate of increase of CAPE is approximately 12% K^{-1} at an SST of 300 K, which is somewhat larger than the rates of increase of 8% K^{-1} [*Muller et al.*, 2011] and 7% K^{-1} [*Romps*, 2011] found in previous studies of RCE. (In the latter publication, this was misstated as being per doubling of CO_2; D. M. Romps, personal communication, 2013).

[9] Figure 1a also shows the cloud-buoyancy integral in each simulation. The cloud-buoyancy integral is a measure of the energy available to convective motions that does not depend on a parcel definition. It is defined to be the vertical integral of the mean buoyancy in cloudy updrafts relative to the domain and time mean. Cloudy updrafts are identified as all points with upward velocity greater than 2 m s^{-1} and cloud water content greater than 0.01 g kg^{-1}, and the integral is taken over all levels for which the mean cloud buoyancy

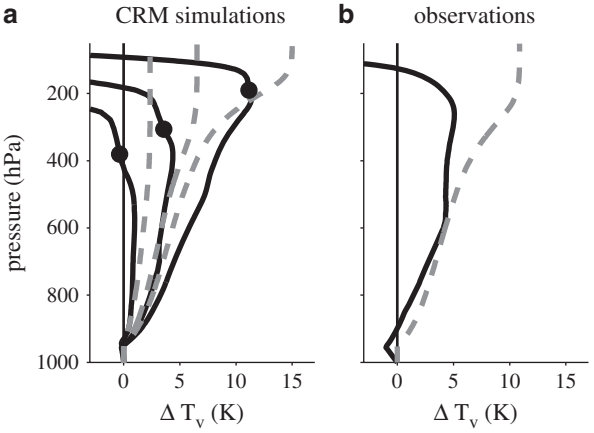

Figure 2. Difference in virtual temperature, ΔT_v, between pseudo-adiabatic parcel ascents and (a) CRM profiles or (b) observed profile (solid) compared with the prediction of ΔT_v from the zero-buoyancy plume model (dashed). In Figure 2a, profiles are based on the time and domain mean of CRM simulations with SSTs of 286, 297, and 309 K (left to right). The LNB is the level at which $\Delta T_v = 0$ in the upper troposphere; the zero-buoyancy plume model does not predict an LNB. Black dots mark the anvil detrainment level as measured by the level of maximum mean ice concentration in the simulations. In Figure 2b, the observational profile is based on the mean over soundings that fall into the red box in Figure 3a, and the parcel and plume are initialized at 1000 hPa.

is positive. The cloud-buoyancy integral also increases with SST, but its absolute value is much smaller than the CAPE, with the CAPE being 5 times larger at the lowest SST and almost 50 times larger at the highest SST (see Figure S3). In the next section, we use this property together with a bulk plume model of convection to better understand why CAPE increases with SST.

3. Zero-Buoyancy Entraining Plume Model

[10] The smallness of the cloud-buoyancy integral relative to the CAPE suggests that some insight may be gained by considering the limit in which clouds are exactly neutrally buoyant with respect to their environment. (This zero-buoyancy limit was previously considered by *Bretherton and Park* [2008] for the case of shallow convection.) We work with an entraining plume as a highly simplified model of an ensemble of convective clouds; similar models are used in many convective parameterizations [e.g., *Tiedtke*, 1989].

3.1. Derivation

[11] First, consider the approximate plume equation,

$$\frac{\mathrm{d}h}{\mathrm{d}z} = -\epsilon(h - h_e), \tag{1}$$

where ϵ is the entrainment rate, $h = c_pT + gz + L_vq_v$ is the moist static energy and the subscript e refers to the environment. Here c_p is the isobaric specific heat capacity of air, L_v is the latent heat of vaporization, T is the temperature, q_v is the specific humidity, g is the gravitational acceleration, and z is height. Ignoring virtual temperature effects, the assumption of neutrality implies $T = T_e$ and thus $h - h_e = L_v(q_v - q_{ve})$. Above cloud base, the plume is saturated such that $h = h^* = h_e^*$ and $q_v = q_v^* = q_{ve}^*$, where an asterisk refers to a quantity at saturation. Using these expressions to evaluate (1) above cloud base gives

$$\frac{\mathrm{d}h_e^*}{\mathrm{d}z} = -\epsilon L_v(q_{ve}^* - q_{ve}). \tag{2}$$

Note that (2) is written only in terms of properties of the environment and the entrainment rate ϵ.

[12] Next, consider an undilute parcel used in the calculation of CAPE that conserves its moist static energy h_u such that $\mathrm{d}h_u/\mathrm{d}z = 0$. Subtracting (2) from the undilute parcel equation gives

$$\frac{\mathrm{d}}{\mathrm{d}z}(h_u^* - h_e^*) = \epsilon L_v(q_{ve}^* - q_{ve}) \tag{3}$$

above cloud base. Assuming for simplicity, a constant entrainment rate and a constant environmental relative humidity $\mathcal{R}_e \simeq q_{ve}/q_{ve}^*$, we may use equation (3) to approximate the temperature difference ΔT between the undilute parcel and the environment. Using the Clausius-Clapeyron equation to linearize the saturation specific humidity about the plume temperature and assuming entrainment acts only above the cloud base z_b, we have that

$$\Delta T(z) \simeq \frac{\epsilon(1-\mathcal{R}_e)}{1 + \frac{L_v}{R_vT^2}\frac{L_vq_{ve}^*}{c_p}} \int_{z_b}^{z} \frac{L_vq_{ve}^*}{c_p}\,\mathrm{d}z', \tag{4}$$

where R_v is the gas constant for water vapor.

[13] The parcel buoyancy is proportional to ΔT, and so equation (4) provides a basis to reason about the behavior of undilute parcel buoyancy and CAPE in an atmosphere that is neutral to an entraining plume. According to (4), the buoyancy of undilute ascent is proportional to the entrainment rate and the relative humidity deficit of the environment $(1 - \mathcal{R}_e)$. Furthermore, as the surface temperature is increased, the integrand in (4) increases in proportion to the mean saturation specific humidity of the troposphere, resulting in larger undilute buoyancy values. At high surface temperatures, the denominator in (4) also plays a role and slows the growth of undilute buoyancy with temperature.

[14] The simple plume model described above highlights the effect of entrainment of dry tropospheric air on the temperature structure of the atmosphere in the zero cloud-buoyancy limit. In what follows, we use a more detailed version of the plume model that takes into account the effects of water on the heat capacity and density of air. The plume equations are integrated upward assuming neutrality with the environment to give a prediction for the vertical profile of environmental temperature which can then be used to calculate CAPE. To crudely account for the bulk effects of many clouds detraining at different levels, we use an entrainment profile of the form $\epsilon(z) = \hat{\epsilon}/z$ [e.g., *Holloway and Neelin*, 2009], while still assuming that entrainment is zero below cloud base (identified here as the lifted condensation level). The other inputs to this zero-buoyancy plume model are the near-surface temperature and specific humidity, and a nominal value for the tropospheric environmental relative humidity. Further details are given in the supporting information (section S2).

3.2. Application to CRM Simulations

[15] The zero-buoyancy plume model reproduces the quasi-exponential increase in CAPE with SST simulated by the CRM (Figure 1a). The plume is initialized with the mean temperature and specific humidity of the lowest model level, and, for simplicity, the environmental relative humidity is taken as 80% at all temperatures and heights. (The free tropospheric relative humidity in the simulations depends on altitude but does not vary greatly from this value.) The zero-buoyancy plume estimate of the environment virtual temperature is only valid up to levels at which convection occurs, and it is always less than that of an undilute parcel. As a result, the zero-buoyancy plume model does not predict the height of the LNB; we instead take as given the LNB diagnosed from the simulations when using the zero-buoyancy plume model to estimate CAPE. The entrainment parameter is set to $\hat{\epsilon} = 0.75$ in order to provide a good overall fit in Figures 1 and 2.

[16] According to the zero-buoyancy plume model, the increase of CAPE with SST in the CRM simulations is largely explained by the combined effects of the increase in the height to which convection extends and the increase in the saturation deficit of the atmosphere leading to more effective reduction of buoyancy by entrainment of dry air. The slight overestimate of CAPE by the zero-buoyancy plume model shown in Figure 1a relates to the LNB being higher than the anvil detrainment level (shown by the dots in Figure 2a) and consequently the assumption of neutral buoyancy not being satisfied at all levels up to the LNB in the integral used to calculate CAPE. Better agreement is found if the upper limit of the CAPE integral is alternatively

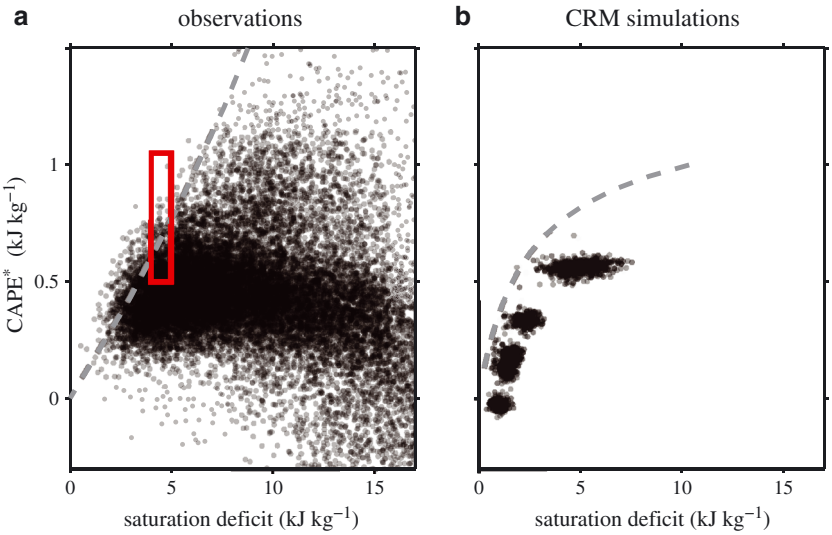

Figure 3. CAPE* for the pressure range 850–400 hPa plotted against the mean saturation deficit over the same layer for (a) radiosonde observations in the tropical western Pacific and (b) grid point columns in the CRM simulations. The saturation deficit ($q_v^* - q_v$) is averaged with mass weighting and multiplied by $L_{v0} = 2.501 \times 10^6$ J kg^{-1} to convert it to energy units. Gray dashed lines correspond to values obtained from the zero-buoyancy plume model with entrainment parameter $\hat{\epsilon} = 1.5$. In Figure 3a, the plume is initialized at saturation with the median temperature of the soundings at 850 hPa and the environmental relative humidity is varied over the range 20%–100%. In Figure 3b, the plume is initialized at saturation with temperatures in the range 261–303 K, and the environmental relative humidity is fixed at 80%.

taken as the level of anvil detrainment in each simulation (Figure 1b).

[17] The results are qualitatively similar for reversible CAPE and no fallout in the zero-buoyancy plume model, although in this case the entrainment parameter must be reduced to $\hat{\epsilon} = 0.5$ to give a good fit to the CRM results (Figure S4) and the buoyancy profiles are somewhat better captured in the upper troposphere (Figure S5). Overall, the increase in CAPE predicted by the zero-buoyancy plume model is slightly smaller than found in the CRM simulations (regardless of assumptions regarding fallout), and this may indicate that the entrainment rate itself increases with temperature. Nevertheless, the quasi-exponential character of the increase in CAPE can be accounted for assuming a fixed entrainment profile.

4. Radiosonde Observations

[18] Since the representation of entrainment in the CRM may not be adequate, we also make a comparison of the zero-buoyancy plume model with radiosonde observations from the tropical western Pacific. To minimize the influence of local boundary-layer fluctuations, we do not consider CAPE based on a surface parcel, but rather CAPE*, which is defined as the integrated buoyancy of a saturated (undilute) parcel lifted pseudo-adiabatically from 850 to 400 hPa. A fixed upper limit is used to allow for a simple comparison with the zero-buoyancy plume model; the value of 400 hPa is chosen to be below the cloud top in the observations and all of the CRM simulations. Neutrality to an entraining plume can only be expected when the atmosphere is convective, and in the case of the observations, the prediction from the zero-buoyancy plume model should be an upper bound on CAPE*. According to the zero-buoyancy plume model, the upper bound on CAPE* will be higher for a drier atmosphere (greater saturation deficit).

4.1. Data

[19] We use temperature and humidity soundings from the level b1 data set of the U.S. Department of Energy Atmospheric Radiation Measurement (ARM) research sites in the tropical western Pacific [*Mather et al.*, 1998]. The ARM data archive contains twice daily, high vertical resolution radiosonde soundings from three stations [Darwin (12.4°S,130.9°E), Manus Island (2.1°S,147.5°E), Nauru (0.5°S,166.9°E)] over the period April 2001 to March 2013. The data are processed in three steps: (1) The soundings are linearly interpolated in pressure onto a uniform grid with a spacing of 5 hPa. Values requiring interpolation between levels more than 20 hPa apart are labeled as missing. (2) Soundings with surface temperatures outside the range 288–313 K are considered to be erroneous and are discarded. Furthermore, temperatures at any level more than 5 standard deviations from the median profile of the resulting subset of soundings are labeled as missing. Any soundings with missing values between 900 and 200 hPa are discarded. (3) Finally, a 1-2-1 temporal filter is applied to ensure the profiles are representative of the atmosphere over a time scale sufficiently long for convective quasi-equilibrium to hold (effectively averaging between daytime and nighttime soundings). The result of this procedure is 19,700 temporally smoothed atmospheric profiles of temperature and humidity which we use in the analysis below.

4.2. Results and Comparison to CRM Simulations

[20] Figure 3a shows the CAPE* based on the pressure range 850–400 hPa plotted against the mean saturation deficit over the same pressure range for each sounding. There is a considerable spread of points, but the upper

left corner is almost completely devoid of soundings, with a strong gradient in the density of points delineating the boundary of this "forbidden" region. There appears to be a limit to the degree of instability that can be maintained in the atmosphere as measured by CAPE*, and the value of CAPE* associated with this limit depends on the midtropospheric saturation deficit such that drier soundings are associated with higher values of CAPE*.

[21] The gray dashed line in Figure 3a shows the position on the scatter plot given by the zero-buoyancy entraining plume model for a range of environmental relative humidities (20%–100%) and initialized with the median temperature of the soundings at 850 hPa and assuming saturation. Relative humidity variations are the major contributor to variations in saturation deficit in the observed soundings (in contrast to the large temperature changes between the CRM simulations). The zero-buoyancy plume model gives a reasonable prediction for the upper bound on CAPE* for a given saturation deficit, although a larger entrainment parameter ($\hat{\epsilon} = 1.5$) is needed as compared to that used in Figures 1 and 2 ($\hat{\epsilon} = 0.75$) since we are now considering the upper bound on CAPE* rather than the mean CAPE.

[22] A similar scatter plot for the CRM simulations is shown in Figure 3b. Here the points correspond to vertical profiles at grid point columns in the model. The profiles are spaced 7 km apart in the horizontal and smoothed with a 1-2-1 filter in time using snapshots 12 h apart. There is less scatter for the simulations compared to the observations because the simulations are of RCE with no large-scale forcing that can stabilize the atmosphere. The clusters of points correspond to simulations with similar SSTs (cf. Figure 1). The prediction from the zero-buoyancy plume model is also shown and gives a reasonable estimate of the upper limit on CAPE* in the simulations. In this case, the zero-buoyancy plume model is initialized with temperatures in the range 261–303 K at 850 hPa (assuming saturation) and with an environmental relative humidity of 80%. Importantly, the same entrainment parameter ($\hat{\epsilon} = 1.5$) is used to match the upper bound on CAPE* for both the observations (Figure 3a) and CRM simulations (Figure 3b).

[23] To examine the vertical profile of buoyancy contributing to CAPE in the observations, we use a subset of radiosonde soundings with relatively high CAPE* and a relative humidity of roughly 80% that is typical of the CRM simulations. The subset is shown by the red box in Figure 3a and includes soundings with CAPE* greater than 500 J kg^{-1} and mean saturation deficits (averaged from 850–400 hPa) between 1.6 and 2 g kg^{-1}. The difference in virtual temperature between a pseudo-adiabatic parcel ascent and the mean of this subset of soundings is shown in Figure 2b, together with the prediction from the zero-buoyancy plume model. The parcel and plume are initialized with the mean temperature and specific humidity at 1000 hPa, and the same entrainment parameter ($\hat{\epsilon} = 0.75$) and environmental relative humidity ($\mathcal{R}_e = 80\%$) are used in the plume as was used in the application to the CRM in Figure 2a. The zero-buoyancy plume model reproduces the magnitude of the observed buoyancy in the lower troposphere but overestimates it in the upper troposphere. This may be partly due to the assumption of total precipitation fallout in the zero-buoyancy plume; the agreement is better when no precipitation fallout is allowed in the plume or parcel ascent (Figure S5).

[24] Overall, the observational results provide support for the CRM simulations and conceptual model discussed here in which lapse rates and CAPE are affected by the tropospheric saturation deficit.

5. Conclusions

[25] We have shown that CAPE increases rapidly with temperature in simulations of RCE over a wide range of SSTs, implying a systematic deviation of the thermal stratification from that of an undilute moist adiabat. The increase in CAPE with SST was accounted for using a conceptual model in which the atmosphere is assumed to be neutrally buoyant with respect to an entraining plume. According to this conceptual model, both the increase in saturation deficit of the troposphere and the increase in height of convection contribute to the increase in CAPE, without the need to invoke a change to the entrainment rate.

[26] Radiosonde observations were used to provide support for the CRM simulations and conceptual model: a measure of CAPE for saturated parcels lifted from 850 to 400 hPa was found to have an upper bound that depends on saturation deficit, and this upper bound could be reproduced by the zero-buoyancy plume model. Importantly, the same entrainment parameters were found to be applicable to both the CRM simulations and the radiosonde observations, despite the difficulty in representing entrainment processes in model simulations.

[27] Further work is needed to understand how our results for RCE relate to changes in CAPE and tropical lapse rates in simulations of the global climate. For small temperature changes, the zero-buoyancy plume model is consistent with the "vertical-shift transformation" of *Singh and O'Gorman* [2012] which has recently been shown to account for much of the intermodel scatter in the response of upper-tropospheric lapse rates to global warming [*O'Gorman and Singh*, 2013]. Climate-model simulations feature increases in CAPE in the tropics [*Sobel and Comargo*, 2011; *Fasullo*, 2012] and increases in the convective contribution to moist available potential energy in the extratropics [*O'Gorman*, 2010], but both of these increases could be influenced by changes in horizontal temperature gradients and circulations in addition to the factors controlling CAPE in RCE.

[28] In our CRM simulations, cloud buoyancy and the vertical velocity of updrafts both increase with SST. Increases in the strength of strong updrafts may be directly tied to the increase in CAPE to the extent that strong updrafts are associated with relatively weak entrainment rates and the distribution of entrainment rates does not change as the SST is increased. However, it is known that cloud updraft velocities also depend on the microphysics of hydrometeor formation and fallout [*Parodi and Emanuel*, 2009], and we leave detailed analysis of the changes in cloud buoyancy and updraft velocity to future work.

[29] **Acknowledgments.** We are grateful to G. Bryan for providing and maintaining CM1 for use by the community. We thank K. Emanuel, Z. Kuang, D. Raymond, and D. Romps for their helpful comments. The radiosonde data were provided by the U.S. Department of Energy as part of the Atmospheric Radiation Measurement (ARM) program. This work was supported by NSF grant AGS-1148594.

[30] The Editor thanks David Romps and an anonymous reviewer for their assistance evaluating this paper.

References

Arakawa, A., and W. H. Schubert (1974), Interaction of a cumulus cloud ensemble with the large-scale environment, part I, *J. Atmos. Sci.*, *31*, 674–701.

Bretherton, C. S., and S. Park (2008), A new bulk shallow-cumulus model and implications for penetrative entrainment feedback on updraft buoyancy, *J. Atmos. Sci.*, *65*, 2174–2193.

Bryan, G. H., and J. M. Fritsch (2002), A benchmark simulation for moist nonhydrostatic numerical models, *Mon. Wea. Rev.*, *130*, 2917–2928.

Derbyshire, S. H., I. Beau, P. Bechtold, J.-Y. Grandpeix, J.-M. Piriou, J.-L. Redelsperger, and P. M. M. Soares (2004), Sensitivity of moist convection to environmental humidity, *Q. J. R. Meteorol. Soc.*, *130*, 3055–3079.

Fasullo, J. (2012), A mechanism for land–ocean contrasts in global monsoon trends in a warming climate, *Clim. Dyn.*, *39*, 1137–1147.

Holloway, C. E., and J. D. Neelin (2009), Moisture vertical structure, column water vapor, and tropical deep convection, *J. Atmos. Sci.*, *66*, 1665–1683.

Kuang, Z., and C. S. Bretherton (2006), A mass-flux scheme view of a high-resolution simulation of a transition from shallow to deep cumulus convection, *J. Atmos. Sci.*, *63*, 1895–1909.

Lin, Y.-L., R. D. Farley, and H. D. Orville (1983), Bulk parameterization of the snow field in a cloud model, *J. Clim. Appl. Meteorol.*, *22*, 1065–1092.

Mather, J. H., T. P. Ackerman, W. E. Clements, F. J. Barnes, M. D. Ivey, L. D. Hatfield, and R. M. Reynolds (1998), An atmospheric radiation and cloud station in the tropical western Pacific, *Bull. Am. Meteorol. Soc.*, *79*, 627–642.

Molinari, J., D. M. Romps, D. Vollaro, and L. Nguyen (2012), CAPE in tropical cyclones, *J. Atmos. Sci.*, *69*, 2452–2463.

Muller, C. J., P. A. O'Gorman, and L. E. Back (2011), Intensification of precipitation extremes with warming in a cloud-resolving model, *J. Clim.*, *24*, 2784–2800.

O'Gorman, P. A. (2010), Understanding the varied response of the extratropical storm tracks to climate change, *Proc. Natl. Acad. Sci.*, *107*, 19,176–19,180.

O'Gorman, P. A., and M. S. Singh (2013), Vertical structure of warming consistent with an upward shift in the middle and upper troposphere, *Geophys. Res. Lett.*, *40*, 1838–1842, doi:10.1002/grl.50328.

Parodi, A., and K. Emanuel (2009), A theory for buoyancy and velocity scales in deep moist convection, *J. Atmos. Sci.*, *66*, 3449–3463.

Riehl, H., and J. S. Malkus (1958), On the heat balance in the equatorial trough zone, *Geophysica*, *6*, 503–538.

Romps, D. M. (2011), Response of tropical precipitation to global warming, *J. Atmos. Sci.*, *68*, 123–138.

Romps, D. M., and Z. Kuang (2010), Do undiluted convective plumes exist in the upper tropical troposphere?, *J. Atmos. Sci.*, *67*, 468–484.

Singh, M. S., and P. A. O'Gorman (2012), Upward shift of the atmospheric general circulation under global warming: Theory and simulations, *J. Clim.*, *25*, 8259–8276.

Sobel, A. H., and S. J. Comargo (2011), Projected future changes in tropical summer climate, *J. Clim.*, *24*, 473–487.

Tiedtke, M. (1989), A comprehensive mass flux scheme for cumulus parameterization in large-scale models, *Mon. Weather Rev.*, *117*, 1779–1800.

Xu, K.-M., and K. A. Emanuel (1989), Is the tropical atmosphere conditionally unstable?, *Mon. Weather Rev.*, *117*, 1471–1479.

Zipser, E. J. (2003), Some views on "hot towers" after 50 years of tropical field programs and two years of TRMM data, *Meteorol. Monogr.*, *29*, 49–58.